IET Renewable Power Generation

Special Issue Call for Papers

Be Seen. Be Cited.
Submit your work to a new IET special issue

Connect with researchers and experts in your field and share knowledge.

Be part of the latest research trends, faster.

Read more

The Institution of Engineering and Technology

Received: 30 December 2022 | Revised: 7 September 2023 | Accepted: 9 October 2023

IET Renewable Power Generation

DOI: 10.1049/rpg2.12867

The Institution of Engineering and Technology WILEY

ORIGINAL RESEARCH

A new approach for harmonic detection based on eliminating oscillatory coupling effects in microgrids

Mojtaba Ahmadi[1] | **Mohammad Hossein Mousavi**[1] | **Hassan Moradi**[1] | **Kumars Rouzbehi**[2]

[1]Department of Electrical Engineering, Razi University, Kermanshah, Iran

[2]Department of System Engineering and Automatic Control, University of Seville, Seville, Spain

Correspondence
Hassan Moradi, Department of Electrical Engineering, Razi University, Kermanshah, Iran.
Email: ha.moradi@razi.ac.ir

Abstract

The primary goal of grid-connected microgrids is to control the active and reactive power, which is reachable by the inner current control loop in the control structure of power converters. However, when facing unbalanced conditions, the inner current control loop implemented in the *dq* frame does not function properly. In such conditions, the popular current control loop malfunctions since there is an oscillatory coupling between harmonic components. Therefore, in this study, a new harmonic detector based on decoupled double synchronous reference frame within the current control loop is proposed in which the oscillatory coupling between harmonic components is eliminated, and the overall performance of the power converter control system is significantly improved. The performance of the precisely developed mathematical models is verified by Matlab simulations, and the simulation results confirm the accuracy and proper operation of the proposed strategy.

1 | INTRODUCTION

In recent years, due to increasing energy consumption, limited fossil fuel resources, and related environmental issues, the use of distributed generation resources has been significantly increased [1]. Despite the numerous benefits associated with microgrids' development, exploiting such grids has always posed challenges, such as, grid synchronization, voltage stability, power quality issues, and being low-inertia by nature that seems to be the root cause of several negative impacts on microgrids [2]. A major issue affecting power quality is harmonics. The presence of harmonics causes larger overall grid losses, increases electrically connected devices and equipment losses, failures in measuring instruments, torque disturbances in electric motors, and perturbations in electronic and telecommunication systems. Hence, the controlling, limiting, and compensating processes for grid harmonics have received immense attention from both industries and researchers [3].

There are effective strategies to compensate the harmonics in microgrids, including harmonic detection and extraction methods [4], primary controllers [5], and secondary controllers [6]. In the first approach, and sometimes even when using the second and third ones, it is necessary to identify and extract harmonics for the purpose of compensation. In other words, harmonic characteristics such as amplitude and phase must be identified using a reliable and accurate method from the main current or voltage signal, and then harmonic components are neutralized within the harmonic compensation strategies. Therefore, the methods of separating and identifying harmonics are of special importance [7].

In general, harmonic isolation and identification can be classified into two groups of frequency-based and time-based methods. In the frequency-based structure, the Fourier series is used to separate the harmonic components from the original signal [8]. Other representations of Fourier series, such as Discrete Fourier Transform (DFT) [9] or Fast Fourier Transform (FFT) as well as Sliding Discrete Fourier Transform (SDFT) [10] are employed in control systems. Neural networks (NNs) or meta-heuristic algorithms are also employed to identify harmonic components. A novel approach for fault diagnosis, utilizing the total harmonic distortion (THD) of the voltage waveform as a key parameter for fault classification has been introduced in [11]. To achieve this, the authors employed a neural network trained with back propagation, genetic algorithm

(GA), and particle swarm optimization (PSO) methods, and subsequently compared their respective outcomes. In [12], a differential harmony search (DHS) algorithm combined with Wavelet Transform (WT) has been used for power quality categorization and to extract distorted signals. The study described in [13] explored a highly effective and economically viable strategy for mitigating harmonics and enhancing the power factor in power distribution networks. This approach involved the application of Shunt Hybrid Active Power Filters (SHAPF) driven by neural network algorithms. In [14], an adaptive harmonic segregation technique has been developed by integrating particle swarm optimization with a deep neural network. All these methods require large memory storage; while some of them do not show a reliable response in the transient state [15, 16] and need precise synchronization methods between the main component and the frequency sampling [17], the others exhibit acceptable transient response [18]. On the other hand, the time-based methods have more speed and less computational burden compared to the frequency-based methods. There are many articles to separate the harmonic components based on the time-based method, including [19], where the instantaneous power theory was exploited. In this article, a high-pass filter was used to identify the harmonics. Other time-based methods benefit from a proportional-resonance (PR) filter or second-order generalized integral filter (SOGI) [20, 21]. Some of these approaches were expanded in the articles and presented under the titles of double (DSOGI) [22], multiple (MSOGI) or SOGI-PLL control algorithm [23] in order to improve the dynamics of the previous methods.

Although the dynamic response waveforms of the $\alpha\beta$-frame PR controller are nearly analogous to the *dq*-frame PI controller when pursuing the positive sequence current references, they are less precise than those of the decoupled *dq*-frame PI scheme [24]. In fact, despite the non-cross-coupled structure of $\alpha\beta$-axes unlike *dq*-axes, the cross-coupling effects between the phase and amplitude of alternative current signals are still witnessed, leading to large transient errors and frequency sensitivity [25]. To overcome this major challenge, [24] has suggested the modified decoupled $\alpha\beta$-frame PR controller and compared it with the decoupled *dq*-frame PI control structure, confirming that both controllers yield similar performance. However, the presence of one more integrator in the $\alpha\beta$-frame PR controller, compared to the decoupled *dq*-frame PI scheme makes its structure more complicated and costly [26].

Besides, unbalanced sequence extraction methods can also be employed, aiming to identify harmonic components. Following *dq* transformation theory, synchronous controllers were implemented using a proportional-integral (PI) controller to segregate unbalanced components [27]. However, this method did not exhibit an optimal performance, so the researchers' attention was drawn to another method called double synchronous reference frame (DSRF), which uses two separate frames to compensate for the unbalanced components. In this strategy, after transferring an unbalanced current or voltage to a synchronous reference frame by employing Park Transformation, a combination of DC component and oscillating components in the voltage or current range is obtained. When this combination passes through a low-pass filter, the oscillating component is removed and ready for using in the current/voltage control loop [28]. However, this approach could not completely eliminate the components of the oscillatory coupling created between the *d* and *q* axes, causing a poor performance of the current control loop and affecting the proper injection of active and reactive power [29]. On the other hand, the strategy can also be presented for the separation of harmonic components. Thus, an SRF-based harmonic detection algorithm was investigated in [30]. This method is used to separate harmonic components, performing the separation process via predetermined compensation angle changes, which has a large computational burden. In [31], this computational load is reduced using BPF as a separator of harmonic components. However, in this approach, only high-order harmonics, that is, $6n \pm 1$ are detected, and dominant harmonics such as 3rd harmonic are not separated. In addition, this method uses BPF, which is a second-order filter that slows down the system, and complicates the calculations. Furthermore, this filter can only separate one harmonic component, in other words, if two harmonic components need to be separated, two BPFs are required. For more components, a group of BPFs must be utilized, which increases the complexity of the control system. To address the weaknesses of the DSRF, a decoupled double synchronous reference frame (DDSRF) was introduced in [32]. Utilizing this enhanced method, the oscillating coupling between unbalanced components was completely eliminated. Moreover, one of the most explored strategies of harmonic detection is active power filters (APFs). Although the harmonic current injection through APFs to suppress the total and selective harmonic currents were studied in the literature [33], the complex configuration and imposing a high cost to the system [34] are yet the most important concerns in some applications.

In this study, firstly, the performance of a DSRF-based controller is investigated facing harmonics in order to highlight its deficiency, then the DSRF system is enhanced, and a harmonic detector based on the DDSRF technique (HD-DDSRF) is presented as a decoupling structure to isolate and eliminate the harmonic fluctuations of the current. In the proposed technique, an unbalanced current vector is defined, which consists of the fifth and seventh harmonic components. Then, this vector is expressed in a DDSRF scheme to identify the harmonic components and remove the oscillatory coupling between them. Furthermore, in this approach, the injection of the current harmonic components is provided by the control loops, and the measured currents are utilized to separate the harmonic components. The contributions of this paper can be listed as follows:

- Accurate identification of harmonic components in the current control system.
- Improving the performance of the current controller using the HD-DDSRF approach.
- Verifying the remarkable performance of the decoupled DSRF method over DSRF in detecting the harmonic components.

The article is organized as follows. In Section 2, the structure of HD-DDSRF is introduced in the presence of harmonic components, and a fair comparison is conducted with DSRF structure. Section 3 presents the case study both for the control structure and power system. Simulation results are illustrated in Section 4. Limitations and future works are stated in Section 5, and finally, a conclusion is given in Section 6.

2 | HD-DDSRF STRUCTURE

Microgrids are designed to operate both in grid-connected and islanded modes. As mentioned before, the main goal of the control system in microgrids connected to the main grid is to properly control active and reactive power. In this case, because the scope of the research is to explore a new harmonic detection system, a constant voltage source has been used instead of DG sources in the studied microgrid. Furthermore, the control system mainly includes the current and voltage control loops. The detailed discussion about microgrid under study and the parameters and the specifications are given in Sections 3 and 4, respectively.

The first step to implementing the current control loop is transferring the three-phase voltage and current vectors into a SRF frame using Park Transformation. Considering balanced condition, these values are DC and without oscillation, in which case the PI controller can provide correct control commands for power control. Conversely, when an unbalanced condition occurs, the voltage and current contain fluctuations leading to disturbing the current control loop [35].

In this section, three-phase vectors are presented in *dq* frame and DSRF technique is introduced while facing harmonics.

Although due to the predominance of 5th and 7th harmonics, it is assumed that the microgrid output current includes the fifth and seventh harmonics, the proposed method has the ability to eliminate other harmonics such as 3rd, 11th etc. in the same way. Here,

$$i_{abc} = i^{h1}_{abc} + i^{h5}_{abc} + i^{h7}_{abc} \tag{1}$$

Due to ease of calculation, the above equation can be expressed in the alpha–beta frame as follows:

$$i_{\alpha\beta} = i^{h1}_{\alpha\beta} + i^{h5}_{\alpha\beta} + i^{h7}_{\alpha\beta} = I^{h1}\begin{bmatrix}\cos(\omega t+\delta)\\ \sin(\omega t+\delta)\end{bmatrix} + I^{h5}\begin{bmatrix}\cos(5\omega t+5\delta)\\ \\ \sin(5\omega t+5\delta)\end{bmatrix} + I^{h7}\begin{bmatrix}\cos(7\omega t+7\delta)\\ \sin(7\omega t+7\delta)\end{bmatrix} \tag{2}$$

where I^{h1}, I^{h5}, I^{h7} are the amplitude of the main, fifth and seventh harmonics, respectively (See also Appendix 1).

In order to present Equation (2) in *dq* frame, Park Transformation is employed as follows [36]:

$$e^{-J\theta} = \begin{bmatrix}\cos(\theta) & \sin(\theta)\\ -\sin(\theta) & \cos(\theta)\end{bmatrix} \tag{3}$$

where

$$\theta = \omega t + \varphi \tag{4}$$

φ represents the phase of θ. Then,

$$\widetilde{i^{1}_{dq}} = e^{-J\theta}\times i_{\alpha\beta} = \begin{bmatrix}\cos(\theta) & \sin(\theta)\\ -\sin(\theta) & \cos(\theta)\end{bmatrix}\times \left(I^{h1}\begin{bmatrix}\cos(\omega t+\delta)\\ \sin(\omega t+\delta)\end{bmatrix} + I^{h5}\begin{bmatrix}\cos(5\omega t+5\delta)\\ \sin(5\omega t+5\delta)\end{bmatrix} + I^{h7}\begin{bmatrix}\cos(7\omega t+7\delta)\\ \sin(7\omega t+7\delta)\end{bmatrix}\right) \tag{5}$$

where $\widetilde{i^{1}_{dq}}$ denotes the current main components in the *dq* frame, which consists of oscillatory terms. Using (4), (5) can be expressed as:

$$\widetilde{i^{1}_{dq}} = I^{h1}\begin{bmatrix}\cos(\varphi-\delta)\\ \sin(\varphi-\delta)\end{bmatrix} + I^{h5}\begin{bmatrix}\cos(4\omega t+4\varphi)\cos(5\varphi-5\delta)+\sin(4\omega t+4\varphi)\sin(5\varphi-5\delta)\\ \sin(4\omega t+4\varphi)\cos(5\varphi-5\delta)-\cos(4\omega t+4\varphi)\sin(5\varphi-5\delta)\end{bmatrix} + I^{h7}\begin{bmatrix}\cos(6\omega t+6\varphi)\cos(7\varphi-7\delta)+\sin(6\omega t+6\varphi)\sin(7\varphi-7\delta)\\ \sin(6\omega t+6\varphi)\cos(7\varphi-7\delta)-\cos(6\omega t+6\varphi)\sin(7\varphi-7\delta)\end{bmatrix} \tag{6}$$

As it is clear from (6), expressions including $\cos(\varphi-\delta)$ and other trigonometric terms whose arc is $(\varphi-\delta)$, represent DC terms because there is no frequency within their arc. Let's assume that:

$$\begin{aligned} i^{h1}_{d} &= I^{h1}\times\cos(\varphi-\delta) \quad , \quad i^{h1}_{q} = I^{h1}\times\sin(\varphi-\delta)\\ i^{h5}_{d} &= I^{h5}\times\cos(5\varphi-5\delta) \quad , \quad i^{h5}_{q} = I^{h5}\times\sin(5\varphi-5\delta)\\ i^{h7}_{d} &= I^{h7}\times\cos(7\varphi-7\delta) \quad , \quad i^{h7}_{q} = I^{h7}\times\sin(7\varphi-7\delta) \end{aligned} \tag{7}$$

where $i^{h1,5,7}_{d,q}$ denotes the DC value of 1st, 5th and 7th harmonics in *dq* frame. Considering (6) and (7),

$$\widetilde{i^{1}_{dq}} = \begin{bmatrix}i^{h1}_{d}\\ i^{h1}_{q}\end{bmatrix} + \begin{bmatrix}i^{h5}_{d}.\cos(4\omega t+4\varphi)+i^{h5}_{q}.\sin(4\omega t+4\varphi)\\ i^{h5}_{d}.\sin(4\omega t+4\varphi)-i^{h5}_{q}.\cos(4\omega t+4\varphi)\end{bmatrix} + \begin{bmatrix}i^{h7}_{d}.\cos(6\omega t+6\varphi)+i^{h7}_{q}.\sin(6\omega t+6\varphi)\\ i^{h7}_{d}.\sin(6\omega t+6\varphi)-i^{h7}_{q}.\cos(6\omega t+6\varphi)\end{bmatrix}$$

$$\rightarrow \widetilde{i^{1}_{dq}} = \underbrace{\begin{bmatrix}i^{h1}_{d}\\ i^{h1}_{q}\end{bmatrix}}_{DC\ term} + \underbrace{\begin{bmatrix}i^{h5}_{d}\\ i^{h5}_{q}\end{bmatrix}}_{DC\ term}\cdot\underbrace{\begin{bmatrix}\cos(4\omega t+4\varphi)+\sin(4\omega t+4\varphi)\\ \sin(4\omega t+4\varphi)-\cos(4\omega t+4\varphi)\end{bmatrix}}_{AC\ term} + \underbrace{\begin{bmatrix}i^{h7}_{d}\\ i^{h7}_{q}\end{bmatrix}}_{DC\ term}\cdot\underbrace{\begin{bmatrix}\cos(6\omega t+6\varphi)+\sin(6\omega t+6\varphi)\\ \sin(6\omega t+6\varphi)-\cos(6\omega t+6\varphi)\end{bmatrix}}_{AC\ term}$$

(8) can be summarized as follows:

$$\widetilde{i^{1}_{dq}} = i^{h1}_{dq} + i^{h5}_{dq}.e^{-J4\theta} + i^{h7}_{dq}.e^{-J6\theta} \tag{9}$$

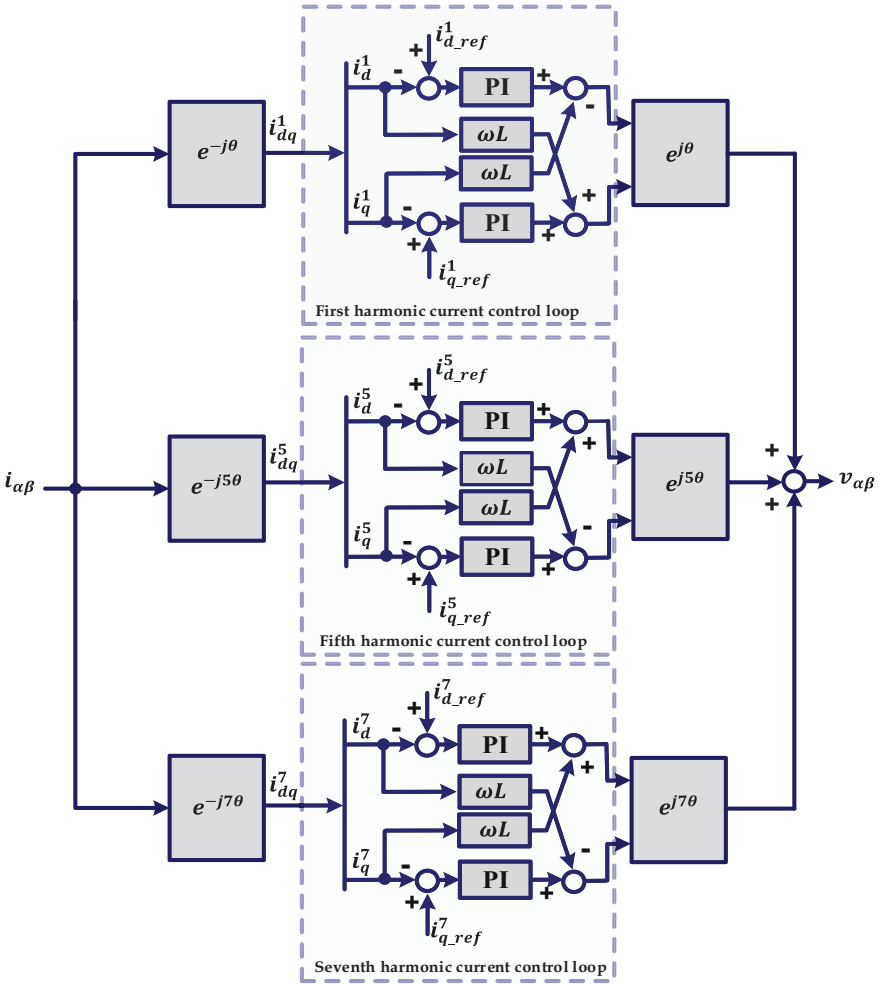

FIGURE 1 Current controller based on DSRF technique.

Similarly, for the fifth and seventh harmonic components:

$$\widetilde{i_{dq}^{5}} = i_{dq}^{b1}.e^{-J4\theta} + i_{dq}^{b5} + i_{dq}^{b7}.e^{-J2\theta} \tag{10}$$

$$\widetilde{i_{dq}^{7}} = i_{dq}^{b1}.e^{-J6\theta} + i_{dq}^{b5}.e^{-J2\theta} + i_{dq}^{b7} \tag{11}$$

From (9)–(11), it is obvious that when the three-phase voltage or current includes harmonics, after transferring to *dq* rotating reference frame, the harmonic components are also transferred to the destination frame. But, the expectation to attain the purely DC values of the *d* and *q* axes is not met, which results in an unfavourable and weak performance of the current control loop. Hence, the DSRF-based current controller can be shown in Figure 1. In order to achieve optimal performance for active and reactive power injection, current fluctuations under unbalanced conditions should be avoided when using DSRF.

To overcome the problems associated with the DSRF technique, here, a new structure called harmonic detector based on the decoupled double synchronous reference frame (HD-DDSRF) is presented in this paper to minimize the fluctuations and their adverse effects.

It can be seen from (9)–(11) that the range of fluctuations in each of the components is dependent on the other two components, so this mutual coupling effect between harmonic components can be eliminated by using the following formulation:

$$i_{dq}^{1} = \underbrace{i_{dq}^{b1}}_{DC\ term} + \underbrace{i_{dq}^{b5}.e^{-J4\theta} + i_{dq}^{b7}.e^{-J6\theta}}_{AC\ term} - \left(\underbrace{i_{dq}^{b5}.e^{-J4\theta} + i_{dq}^{b7}.e^{-J6\theta}}_{Cross-coupling\ term} \right) \tag{12}$$

$$i_{dq}^{5} = \underbrace{i_{dq}^{b5}}_{DC\ term} + \underbrace{i_{dq}^{b1}.e^{-J4\theta} + i_{dq}^{b7}.e^{-J2\theta}}_{AC\ term} - \left(\underbrace{i_{dq}^{b1}.e^{-J4\theta} + i_{dq}^{b7}.e^{-J2\theta}}_{Cross-coupling\ term} \right) \tag{13}$$

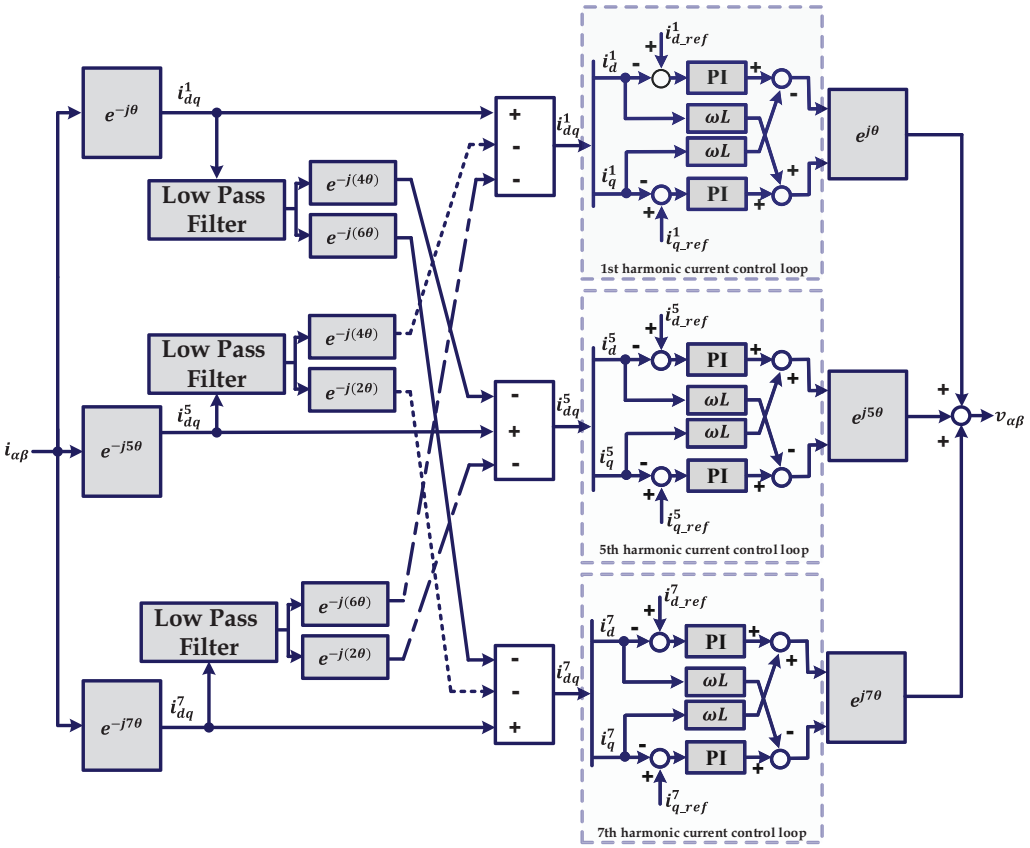

FIGURE 2 Current controller based on proposed HD-DDSRF technique.

$$i^7_{dq} = \underbrace{i^{h7}_{dq}}_{DC\ term} + \underbrace{i^{h1}_{dq}.e^{-J6\theta} + i^{h5}_{dq}.e^{-J2\theta}}_{AC\ term} - \left(\underbrace{i^{h1}_{dq}.e^{-J6\theta} + i^{h5}_{dq}.e^{-J2\theta}}_{Cross-coupling\ term}\right) \tag{14}$$

where $i^{1,5,7}_{dq}$ shows the output HD-DDSRF in dq frame.

In fact, in this strategy, the oscillating terms of the other harmonic components are created and subtracted from the original term to eliminate the coupling effects. Figure 2 illustrates the structure of the proposed HD-DDSRF.

3 | MICROGRID UNDER STUDY AND THE PROPOSED CONTROL SYSTEM

Figure 3 shows the generalized structure of a distributed generation unit which is connected to the main grid through an LC filter along with the control system. As can be seen from the figure, a current controller based on HD-DDSRF is proposed to control the active and reactive power in the dq frame.

Three current controllers have been used to inject harmonic components. When the harmonic components are completely separated by HD-DDSRF technique, they are now ready to be used in the current control loop. By employing KVL in the output filter of the distributed generation unit and transferring the relevant equations to the dq frame by using the HD-DDSRF, the following equations are obtained:

$$L\frac{di^{h1}_d(t)}{dt} + (R + r_{on})\, i^{h1}_d(t) = V^{h1}_{td}(t) + V^{h1}_{gd}(t) + L\omega_0 i^{h1}_q(t) \tag{15}$$

$$L\frac{di^{h1}_q(t)}{dt} + (R + r_{on})\, i^{h1}_q(t) = V^{h1}_{tq}(t) - V^{h1}_{gq}(t) - L\omega_0 i^{h1}_d(t) \tag{16}$$

$$L\frac{di^{h5}_d(t)}{dt} + (R + r_{on})\, i^{h5}_d(t) = V^{h5}_{td}(t) + V^{h5}_{gd}(t) + L\omega_0 i^{h5}_q(t) \tag{17}$$

$$L\frac{di^{h5}_q(t)}{dt} + (R + r_{on})\, i^{h5}_q(t) = V^{h5}_{tq}(t) - V^{h5}_{gq}(t) - L\omega_0 i^{h5}_d(t) \tag{18}$$

$$L\frac{di^{h7}_d(t)}{dt} + (R + r_{on})\, i^{h7}_d(t) = V^{h7}_{td}(t) + V^{h7}_{gd}(t) + L\omega_0 i^{h7}_q(t) \tag{19}$$

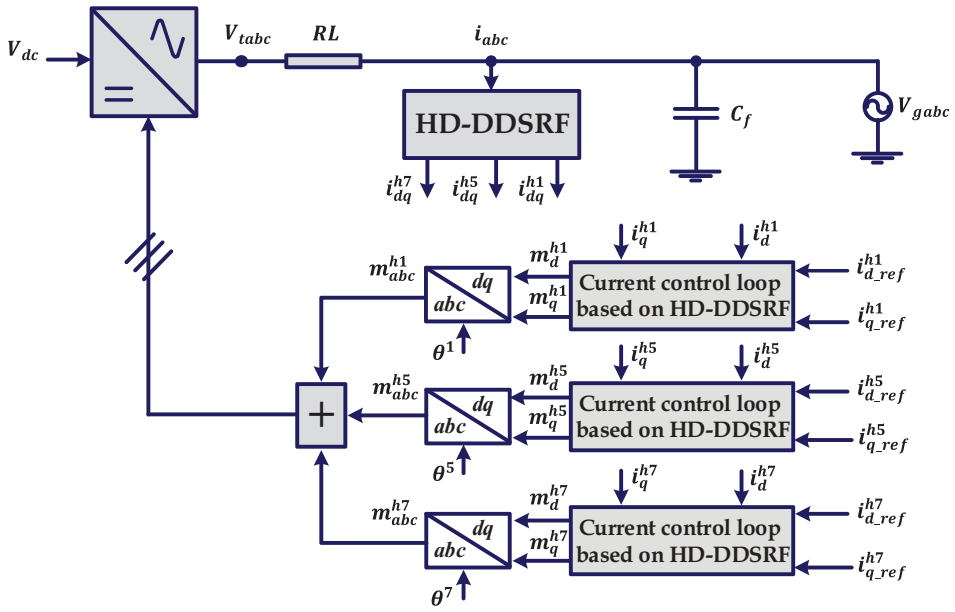

FIGURE 3 Schematic of distributed generation unit under study.

TABLE 1 Specifications of the system under study.

Parameters	Value	Unit
Peak phase voltage	311	[V]
DC-link voltage	650	[V]
Grid frequency	50	[Hz]
Switching frequency	10	[kHz]
Inductance	1.8	[mH]
Capacitance	25	[μF]
Resistance	1.19	[mΩ]
Switch resistance	0.88	[mΩ]
Filter damping ratio	0.707	–

$$L\frac{di_q^{h7}(t)}{dt} + (R + r_{on})\, i_q^{h7}(t) = V_{tq}^{h7}(t) - V_{gq}^{h7}(t) - L\omega_0 i_d^{h7}(t) \tag{20}$$

where

$$V_{tdq}^{h1,5,7}(t) = \frac{V_{dc}}{2} m_{dq}^{h1,5,7} \tag{21}$$

R and L are the resistance and inductance of output filter, respectively. r_{on} denotes switch internal resistance and ω_0 is grid frequency. Also, V_t, V_{dc} and m_{dq} sequentially denote inverter terminal voltage, inverter DC side voltage, and control command applied to the inverter gate. Equations (15)–(20) show that there is a coupling between I_d and I_q in the harmonic sequences. To remove this coupling, according to Figure 4, a feed-forward compensator is applied.

According to Figure 5, to design the controllers, the simplified block diagram of the current sequences closed-loop control system is considered. PI controller is implemented to equalize the steady state error of the closed loop system to zero. Thus,

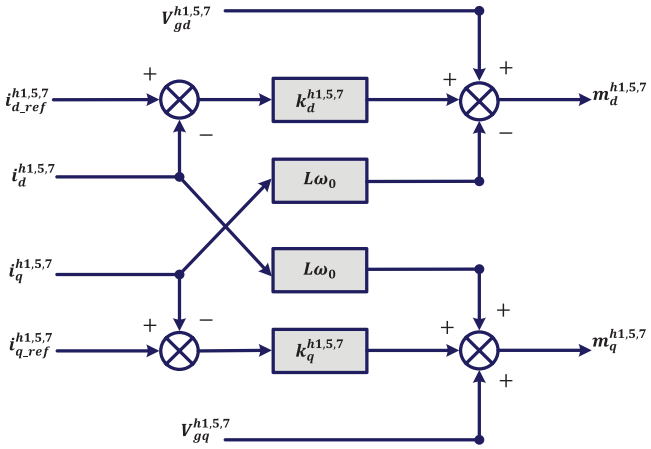

FIGURE 4 Block diagram of harmonic sequences current controllers based on HD-DDSRF.

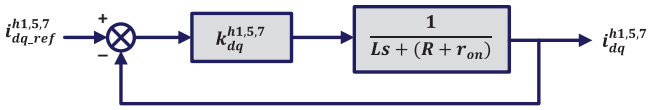

FIGURE 5 Simplified block diagram of closed-loop current control system based on HD-DDSRF for LCL filter.

$$k_{d,qI}^{h1,5,7} = k_p + \frac{k_i}{s} \tag{22}$$

$k_{d.qI}^{h1.5.7}$ represents the coefficients of PI controllers for the 1st, 5th and 7th harmonics in d-q frame. k_p and k_i are the pro-

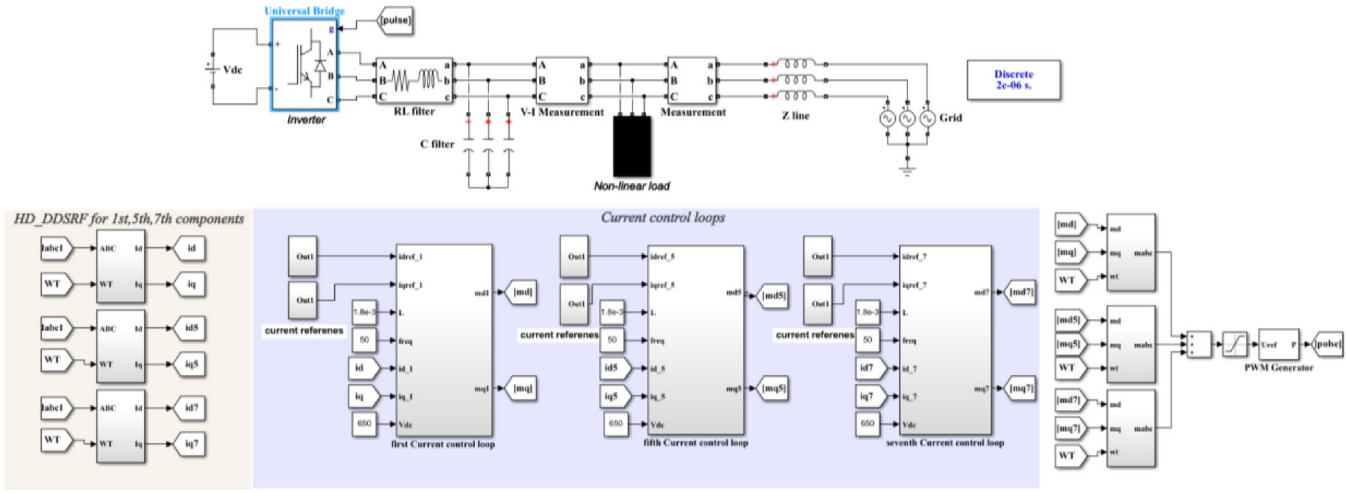

FIGURE 6 MATLAB schematic of simulation scenarios.

TABLE 2 Scenario one specifications.

Current references injection time	Harmonic component	Current amplitude
$t = 0.8$ s	$b1$- d axis	4 A
$t = 1$ s	$b1$-q axis	−2 A
$t = 1.1$ s	$b5$- d axis	−1 A
$t = 1.2$ s	$b5$- q axis	2 A
$t = 1.3$ s	$b7$- d axis	2 A
$t = 1.4$ s	$b7$- q axis	−1 A

portional and integral coefficients, respectively. The open loop transfer function of the current control system is as follows:

$$T_{oli}(s) = \left(\frac{k_p}{Ls}\right)\left(\frac{s + \frac{k_i}{k_p}}{s + \frac{R+r_{on}}{L}}\right) \tag{23}$$

Based on (23), the open loop transfer function has a pole close to the origin.

The zero of the PI controller is selected to eliminate this pole. Then:

$$\frac{k_i}{k_p} = \frac{R + r_{on}}{L} \tag{24}$$

Finally, the closed-loop transfer function of the current control system can be written as follows:

$$G_i(s) = \frac{i_{d,q}^{b1,5,7}(s)}{i_{d,q\ ref}^{b1,5,7}(s)} = \frac{1}{\tau_i s + 1} \tag{25}$$

where τ_i indicates the time constant of the closed loop system:

$$\frac{k_p}{L} = \frac{1}{\tau_i} \tag{26}$$

To achieve a fast system response, τ_i should be small and for this purpose, according to (26), a large value for k_p should be adopted.

On the other hand, according to (25), the closed loop system of current control acts like a first-order low-pass filter; hence, by reducing τ_i (increasing the value of k_p), the bandwidth of the closed loop control system increases.

To control active and reactive power, according to instantaneous power theory in the dq frame for fundamental components [37]:

$$P_s^1(t) = \frac{3}{2}\left[V_d^1(t)\, i_d^1(t) + V_q^1(t)\, i_q^1(t)\right] \tag{27}$$

$$Q_s^1(t) = \frac{3}{2}\left[-V_d^1(t)\, i_q^1(t) + V_q^1(t)\, i_d^1(t)\right] \tag{28}$$

If the PLL is in the steady-state $V_q^1 \approx 0$that is why:

$$P_s^1(t) = \frac{3}{2}\left[V_d^1(t)\, i_d^1(t)\right] \tag{29}$$

$$Q_s^1(t) = \frac{3}{2}\left[-V_d^1(t)\, i_q^1(t)\right] \tag{30}$$

Therefor based on above equations P_s^1 and Q_s^1 can be controlled by i_d^1 and i_q^1 respectively, thus:

$$i_{dref}^1(t) = \frac{2}{3V_d^1} P_s^1(t) \tag{31}$$

$$i_{qref}^1(t) = \frac{-2}{3V_d^1} Q_s^1(t) \tag{32}$$

The above equations state that changes in the current references will result in changes in the active and reactive power loop.

4 | SIMULATION RESULTS

The system shown in Figure 3 has been simulated using the Simscape toolbox in Matlab/Simulink. To evaluate the effectiveness of the proposed HD-DDSRF method, it is compared with DSRF approach.

Two scenarios have been simulated in this study. For the first scenario, variation of current references at different times is considered to create harmonic currents in the inverter output. The specifications of the studied system components are listed in Table 1.

In the second scenario, to show the robustness of the proposed detection scheme under harsh harmonic conditions, in addition to reference harmonic current injection, a nonlinear load [38] has been added to the system. Figure 6 illustrates the MATLAB schematic of simulated scenarios.

4.1 | Scenario 1

In this scenario, to evaluate the performance of HD-DDSRF in harmonic component detection and control, the reference values are changed from zero to the determined values presented in Table 2.

The simulation first scenario while injecting harmonic components are expressed as follows:

Figure 7 shows the current of main harmonic component in *d* and *q* axes for both methods. As can be seen, after applying the reference values at $t = 1.1$ s and $t = 1.3$ s for the 5th harmonic as well as $t = 1.2$ s and $t = 1.4$ s for the 7th harmonic in both *d* and *q* axes, the main component current in *d*-axis follows its reference value which is 4 A. There is also a same trend in the *q*-axis. It is clear that the control method based on DSRF exhibits a wide range of oscillations in both *dq* axes leading to weak performance of current controllers in injecting active and reactive power, according to Figure 8.

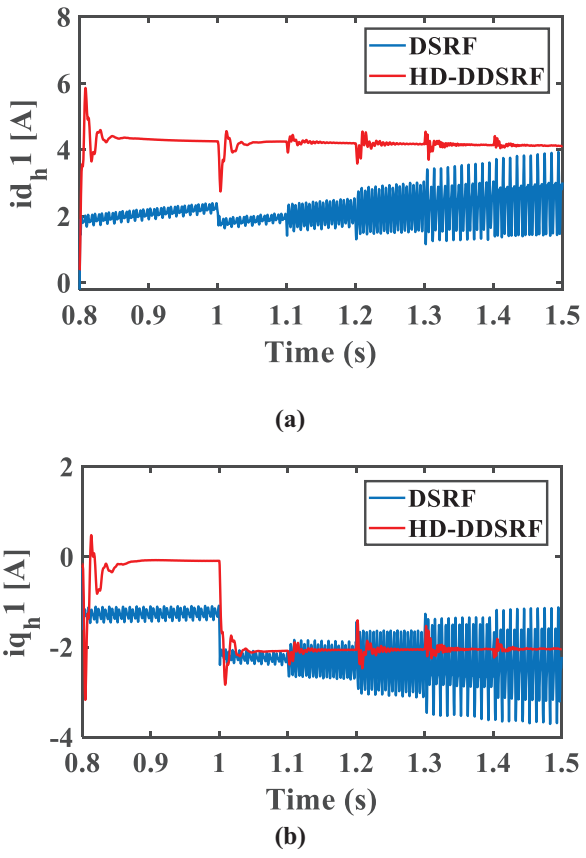

FIGURE 7 Main component current waveform (a) *d*-axis with $i_{dref}^{h1} = 4$ A at $t = 0.8$ s, (b) *q*-axis with $i_{qref}^{h1} = -2$ A at $t = 1$ s.

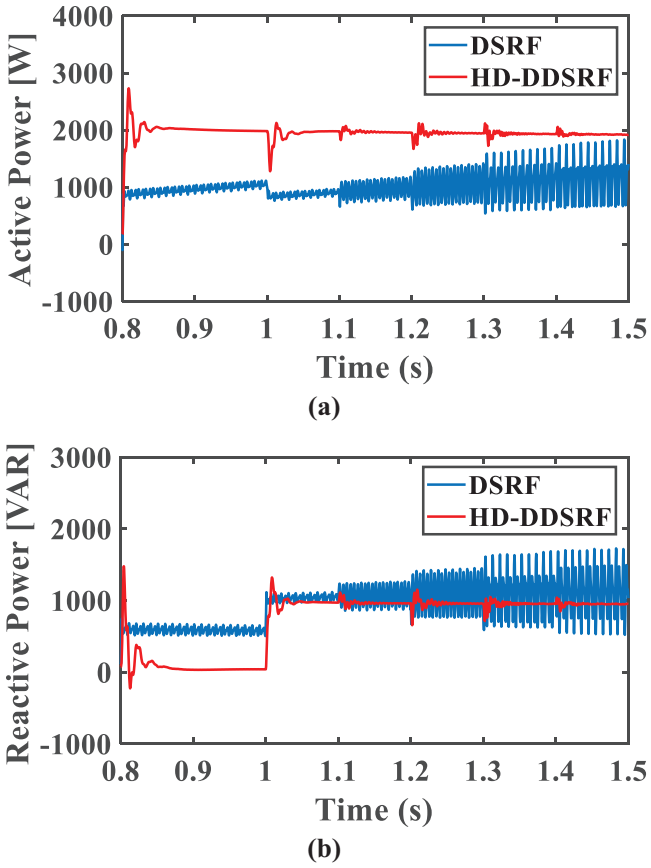

FIGURE 8 Injected power for both DSRF and HD-DDSRF methods: (a) active, (b) reactive.

In the *d*–*q* frame, the current signals are not purely DC and contain oscillations with frequencies of 2ω, 4ω and 6ω. Hence, using FFT analysis, a new definition is presented to display the frequency spectrum as an index relative the DC components of the signal, called Magnitude of DC% (shown as THD% in the graphs). Here, to maintain MATLAB standard FFT analysis outputs, magnitude of DC is shown as THD% in the figures, but they differ from three-phase THD% definition. This THD% shows the oscillations in DC signals. In order to compare the range of these oscillations, the current harmonic spectrum is depicted in Figure 9. As can be observed, the magnitude of DC%, when using DSRF-based controller in *d* and *q* axes, is 38.06% and 23.02%, respectively. In addition, the sixth and fourth harmonics have appeared in the *dq* frame, which can be proved using (12). The suggested HD-DDSRF control structure reduces the range of other component variations on the main harmonic and guarantees the proper injection of active and reactive power. According to Figure 10, the magnitude of

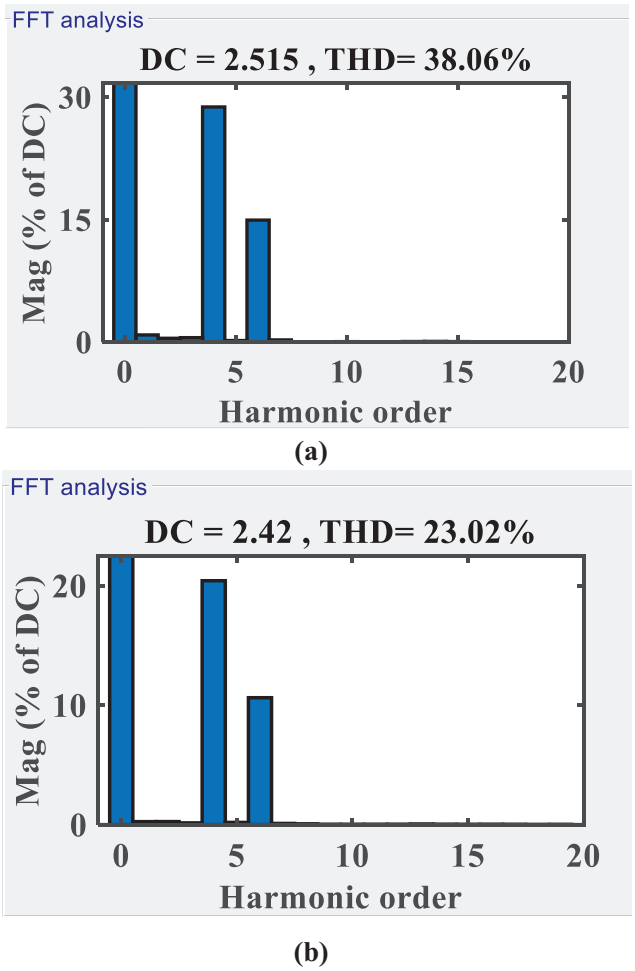

FIGURE 9 The harmonic spectrum of the main component current when using DSRF method: (a) *d*-axis, (b) *q*-axis.

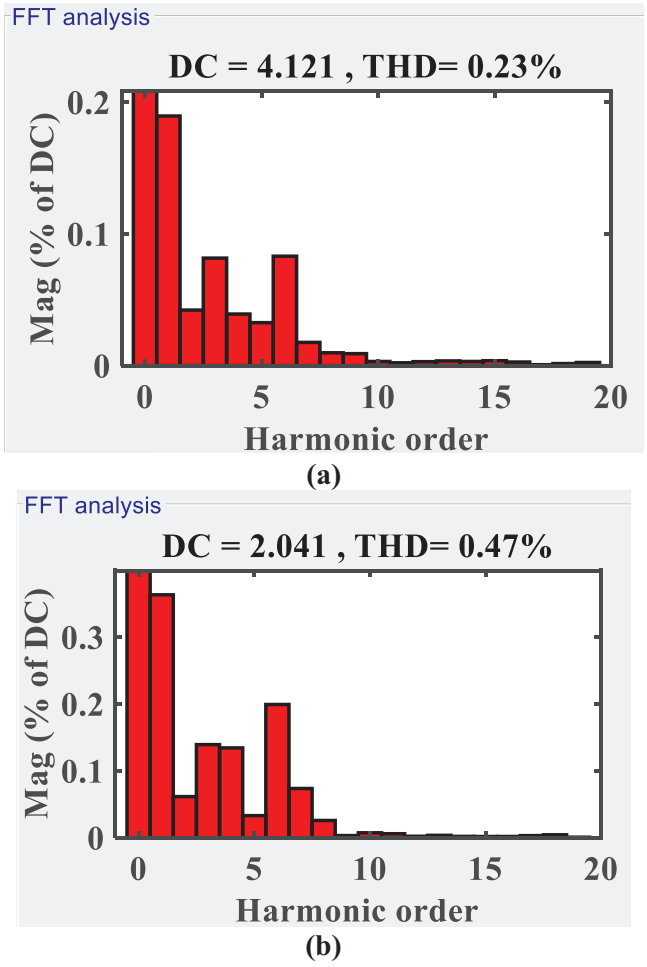

FIGURE 10 The harmonic spectrum of the main component current when using HD-DDSRF method: (a) *d*-axis, (b) *q*-axis.

DC% for HD-DDSRF in *d* and *q* axes is 0.23% and 0.47%, respectively. It should be noted that all MoDC values are in an acceptable range.

As mentioned, such a process can be employed to achieve the pure DC values of the 5th and 7th harmonic components. For this purpose, if the output current of the inverter is transferred to the *d*–*q* axis with a frequency of 5 or 7 times the main frequency and other components do not inject any current, the *dq* current is free of oscillations for both harmonic components. But when the current references of other components change, an oscillating couple with a significant amplitude is created. In this situation, similar to the main harmonic component waveforms, the DSRF-based method fails to remove fluctuations, resulting in a slower system performance. As is observed from Figure 11, when the current reference of the main component is applied at $t = 0.8$ s and $t = 1$ s as well as the current reference of the 7th component at $t = 1.3$ s and $t = 1.4$ s in the *dq* axes, by using DSRF technique, oscillating amplitudes, or in other words, oscillatory coupling, are created between the 5th harmonic components, and it shows that this method does not hold the required efficiency.

The effectiveness of the proposed HD-DDSRF method is clearly demonstrated in its ability to proficiently decouple components and eliminate oscillatory effects originating from other components. A similar trend exists for the 7th harmonic (Figure 12).

Figures 13–16 demonstrate the harmonic spectrum of current in *dq* axes for 5th and 7th components. Referring to Figures 13 and 14, the DSRF magnitude of DC% value is equal to 37.07% and 20.82% for the 5th harmonic in the *d* and *q* axis, which are significantly decreased to 1.48% and 0.86% after using the proposed HD-DDSRF (Figure 14).

Furthermore, from Figure 15, the magnitude of DC% value of the 7th component after transferring to the *dq* axis using DSRF-based method is equal to 16.46% and 75.79% for *d* and *q* axes, which is far beyond its allowed limit, while in the proposed HD-DDSRF method According to Figure 16, the magnitude of DC% value reaches 0.32% and 0.77% for *d* and *q* axes, respectively.

Following the above discussion, it can be concluded that the HD-DDSRF method completely and effectively eliminates the fluctuations caused by the coupling of the components to each other (mutual coupling effect), and in all cases the magnitude of

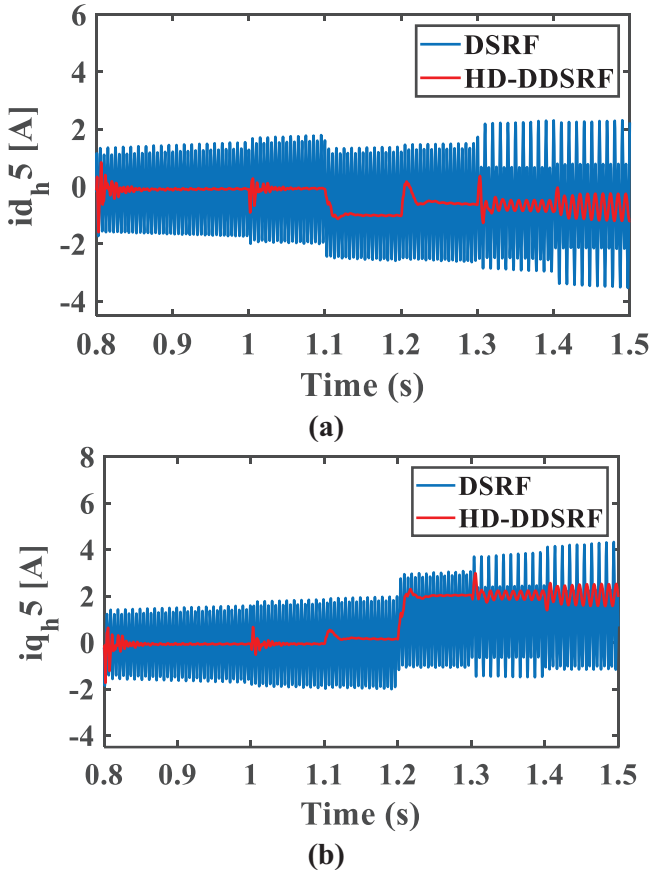

FIGURE 11 Fifth component current waveform. (a) *d*-axis with $i_{dref}^{h5} = -1$ A at $t = 1.1$ s, (b) *q*-axis with $i_{qref}^{h5} = 2$ A at $t = 1.2$ s.

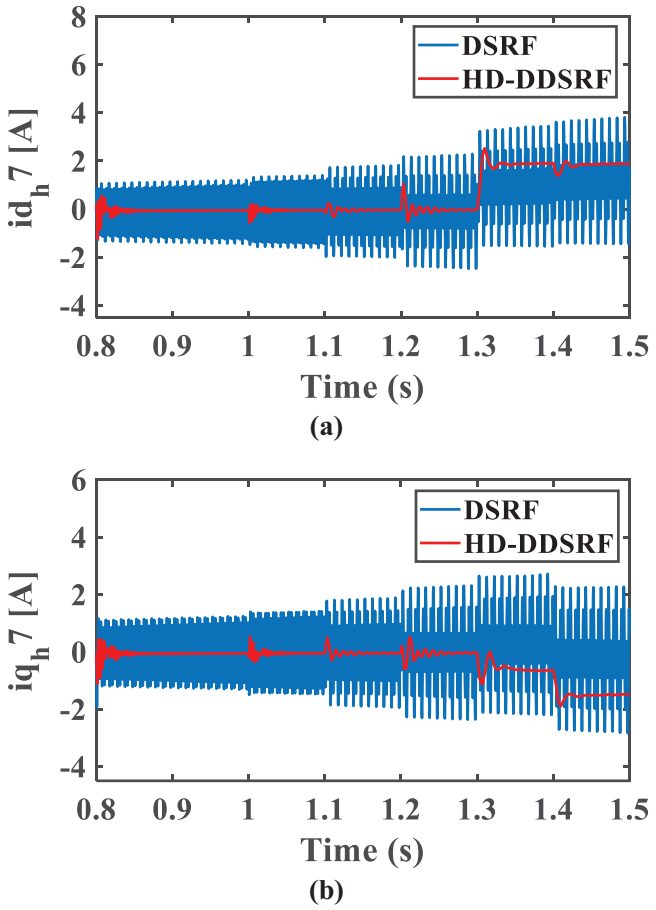

FIGURE 12 Seventh component current waveform. (a) *d*-axis with $i_{dref}^{h7} = 2$ A at $t = 1.3$ s, (b) *q*-axis with $i_{qref}^{h7} = -1$ A at $t = 1.4$ s.

DC% value is in an acceptable range. This is a confirmation of the proper operation of the proposed control system based on HD-DDSRF.

4.2 | Scenario 2

n this scenario, aiming to show the flexibility and robustness of the proposed detection method, a worse harmonic condition is considered. A combination of reference harmonic current injection and a nonlinear load has been simulated. The characteristics of the nonlinear load and the scenario 2 specifications are presented in Table 3.

As can be observed from Figure 17, until $t = 0.4$ s, the reference current of 5th harmonic is equal to zero. After $t = 0.4$ s, when the nonlinear load (containing 5th and 7th harmonics) is added, the 5th harmonic current amplitude is increased to reach almost 20 A and 15 A for the *d* and *q* axes, respectively. Due to the current reference value remaining at zero during time intervals $t = 1.3$ s and $t = 1.4$ s (as indicated in Table 3), the amplitude of this harmonic component diminishes to zero within a brief period. Therefore, the change in the references at $t = 1.3$ s and $t = 1.4$ s for *d* and *q* axes will be tracked.

Based on the information extracted from Figure 18, it is evident that the reference current for the 7th harmonic remains at zero until $t = 0.4$ s. Subsequently, upon introducing the nonlinear load, the amplitude of the 7th harmonic current increases and reaches nearly 20 A for *dq* axes. Despite this, the current reference value continues to remain zero until $t = 1.5$ s and $t = 1.6$ s. Consequently, the amplitude of this specific harmonic component returns to zero after a brief interval, signifying the potential

TABLE 3 Scenario two specifications.

Current references injection time	Harmonic component	Current amplitude
$t = 1$ s	*h*1- *d* axis	4 A
$t = 1.2$ s	*h*1-*q* axis	−2 A
$t = 1.3$ s	*h*5- *d* axis	−1 A
$t = 1.4$ s	*h*5- *q* axis	2 A
$t = 1.5$ s	*h*7- *d* axis	2 A
$t = 1.6$ s	*h*7- *q* axis	−1 A
Nonlinear load		
$R = 100\ \Omega$	$L = 84\ \mu$H	$C = 235\ \mu$F
Applied at $t = 0.4$ s		

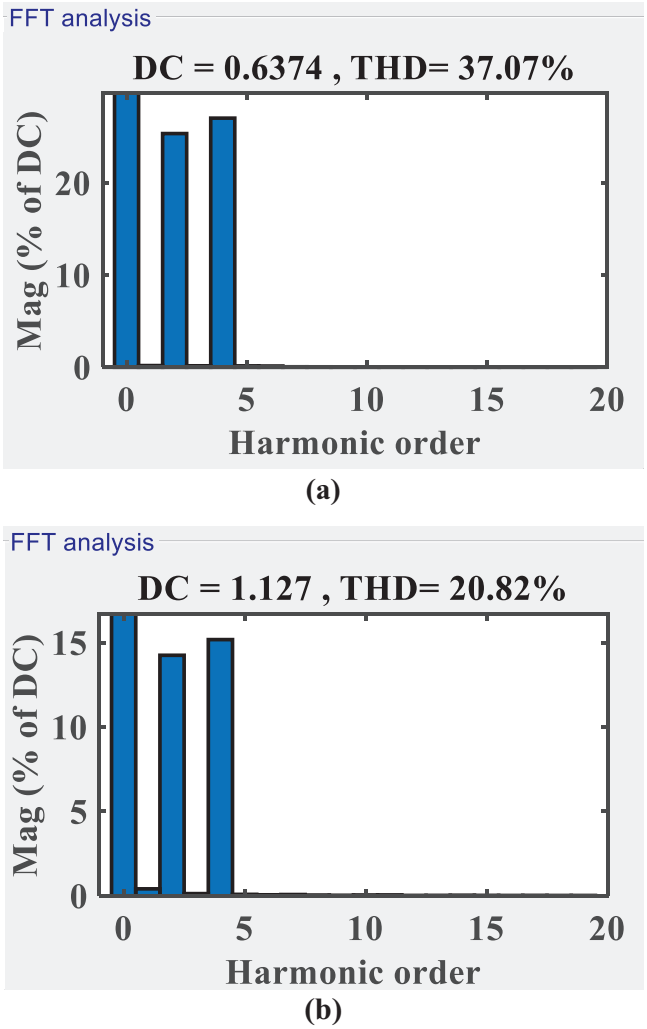

FIGURE 13 The harmonic spectrum of the 5th component current when using DSRF method: (a) *d*-axis, (b) *q*-axis.

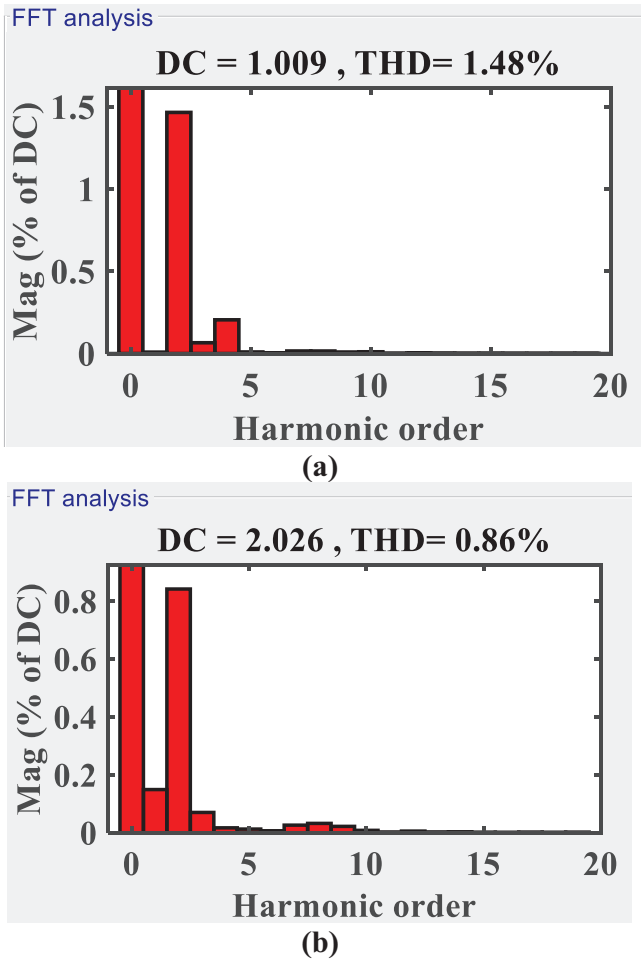

FIGURE 14 The harmonic spectrum of the 5th component current when using HD-DDSRF method: (a) *d*-axis, (b) *q*-axis.

for control over the harmonic component. As a result, the references values get to 2 and −1 A for both axes accordingly.

The bar charts shown in Figures 19 and 20 present the harmonic spectrum of current in the *dq* axes, specifically focusing on the 5th and 7th components. These figures represent the response under a nonlinear load condition and variations in the reference values. Overall, these bar charts effectively highlight the results of the FFT analysis, allowing for a quick assessment of the distribution and prominence of the DC value within the analyzed signal frequency spectrum.

Referring to Figure 19, it can be observed that the magnitude of DC% values for the 5th harmonic in the *d* and *q* axes are 6.21%and 5.27%, respectively. These values are significantly lower than those achieved using the DSRF method, even under undesired conditions. Similarly, for the 7th harmonic, the magnitude of DC% values in the *d* and *q* axes are 4.32% and 4.8% respectively, which are considered as acceptable outputs (Figure 20). These results solidify the efficacy of the proposed method in effectively managing severe harmonic conditions and highlight its potential to outperform traditional approaches.

Overall, the key function of the proposed HD-DDSRF method is to detect the harmonic orders and supress the amplitude of AC oscillations within DC signals. Meaning that, the amplitude of harmonic orders can be identified more precisely than DSRF technique. For instance, from Figure 20, besides detecting the seventh harmonic (frequency of 7ω), other harmonics may exist that the magnitude of them are about 4%.

5 | COMPARISON WITH IEEE-519 STANDARD

In previous section, it was shown that the proposed HD-DDSRF technique is very effective in detecting almost pure harmonics through mitigating the oscillations. On the other hand, there is no standard limits in *dq* axis for a fair comparison. In this section, to demonstrate the effectiveness of the proposed technique clearly, the *dq* harmonic waveforms are transferred to *ABC* frame to be compared with IEEE-519 standards [39]. Derived from this standard, for $2 \leq h < 11$, the maximum permitted total harmonic distortion (THD %) is 4%.

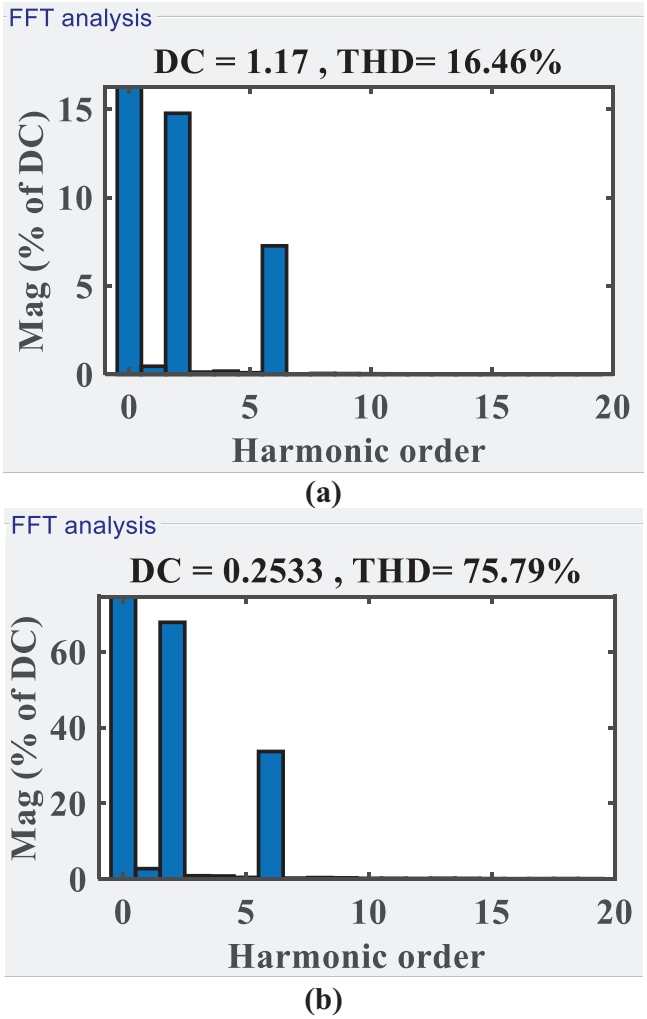

FIGURE 15 The harmonic spectrum of the 7th component current when using DSRF method: (a) *d*-axis, (b) *q*-axis.

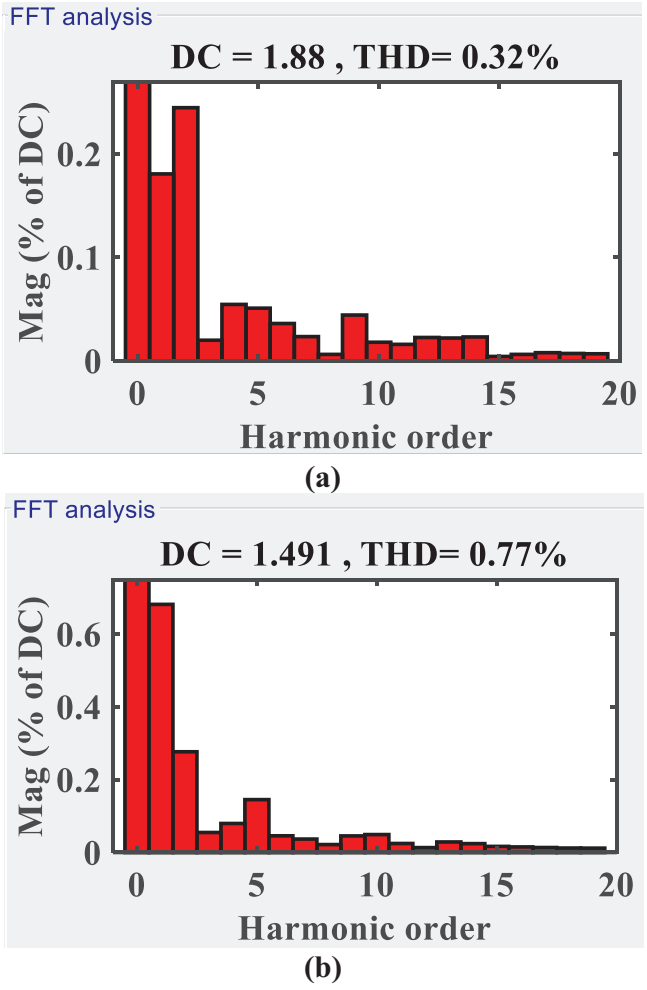

FIGURE 16 The harmonic spectrum of the 7th component current when using HD-DDSRF method: (a) *d*-axis, (b) *q*-axis.

According to the results extracted from the simulation scenarios, it was found that the proposed method identifies and eliminates the oscillations in the *dq* frame with very high precision. But as mentioned, there is no standard for measuring the permissible number of oscillations in the *dq* frame. Thus, in this section, the outputs of the DSRF method as well as the proposed technique for the first, fifth and seventh harmonic components are separately transferred to the *ABC* frame. Then, in order to check the efficiency of the presented methods, their THD % values in the *ABC* frame are investigated. The reason for separately transferring the first, fifth and seventh components to the three-phase frame is that the method presented in this paper is a harmonic detection technique and it should be verified that how precise this detection technique is over other approaches.

Figures 21a and 21b respectively represent the three-phase currents of the main component resulting from the DSRF and the proposed method (HD-DDSRF). As it is clear from the Figure 21c,d, after transferring the signals from the *dq* frame to the *ABC*, the oscillations are not well-damped in the DSRF method and these oscillations are referred to the three-phase frame. Clearly, the THD value reaches 27%, which is about 23% more than the allowed value of 4% for distribution networks according to the IEEE standard. On the other hand, it can be seen that the oscillations in the *dq* frame are well-suppressed in the proposed method, so that after transferring to the *ABC* frame, the THD value is limited to below 2% (within the standard range). In other words, the proposed method has been able to identify the main harmonic components with high accuracy.

Figures 22a and 22b show the three-phase waveforms of the fifth component current for both DSRF and DDSRF methods. These figures have a frequency of 5ω. As it is observed, the waveform resulting from the DSRF method contains harmonics or frequencies other than 5ω. According to Figure 22c, which exhibit the FFT analysis, it is evident that in the DSRF method, the THD value of DSRF method is equal to 66%. This indicates that this method, in addition to detecting the 5ω frequency, the other frequencies are also passed. It shows the inaccuracy of this method. On the other hand, according to Figure 22d, the HD-DDSRF THD value, 0.81%, is within its standard range (4%), and according to the previous analysis,

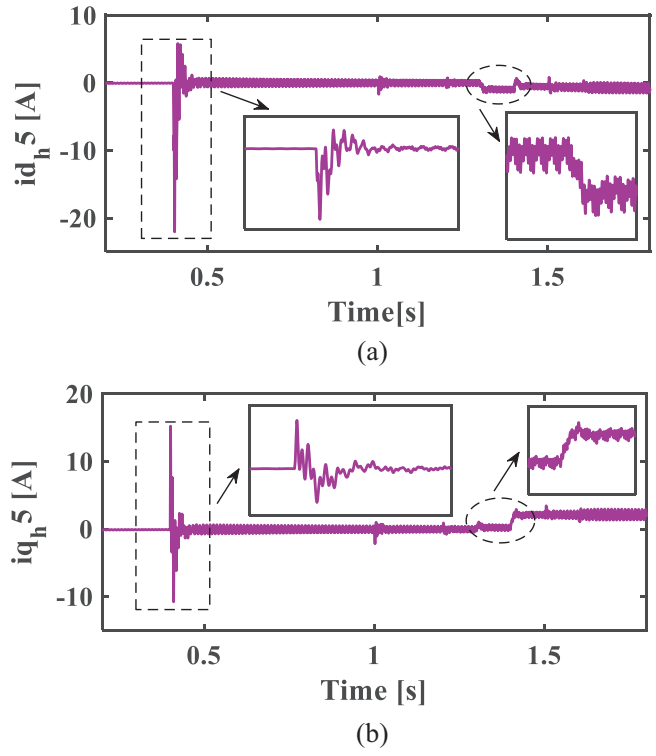

FIGURE 17 Fifth component current waveform. (a) *d*-axis with $i^{h5}_{dref} = -1$ A at $t = 1.3$ s, (b) *q*-axis with $i^{h5}_{qref} = 2$ A at $t = 1.4$ s.

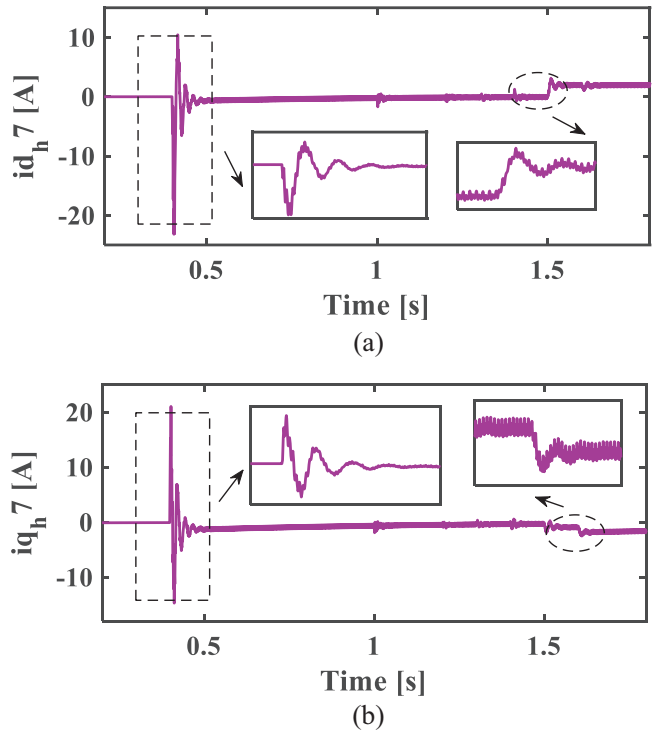

FIGURE 18 Seventh component current waveform. (a) *d*-axis with $i^{h7}_{dref} = 2$ A at $t = 1.5$ s, (b) *q*-axis with $i^{h7}_{qref} = -1$ A at $t = 1.6$ s.

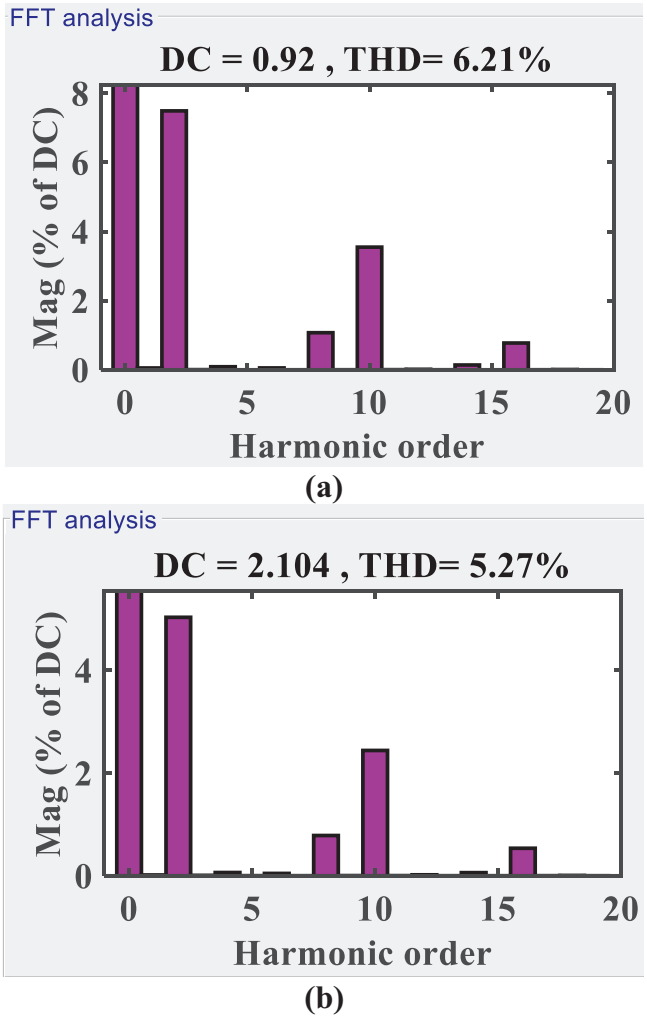

FIGURE 19 The harmonic spectrum of the 5th component current when using HD-DDSRF method: (a) *d*-axis, (b) *q*-axis.

it means that only 5ω harmonics are detected and allowed to be transferred into *ABC* frame. Same pattern is true for seventh harmonic. As shown in Figure 23, the THD value related to DSRF and HD-DDSRF for this component is 46.2% and 2.56%, respectively.

Also, for scenario B, which considered more harsh harmonic conditions, by transferring the signals from the *dq* axis to the three-phase axis, it can be witnessed that the THD values of the proposed method for the 5th and 7th harmonics are equal to 4.72% and 2.75%. Considering that the severe harmonic circumstances were applied in this scenario, but the values of THD are close to the standard range (Figure 24).

6 | LIMITATIONS AND FUTURE WORKS

Through a fair comparison between DSRF and HD-DDSRF methods, a clear understanding of the benefits and drawbacks

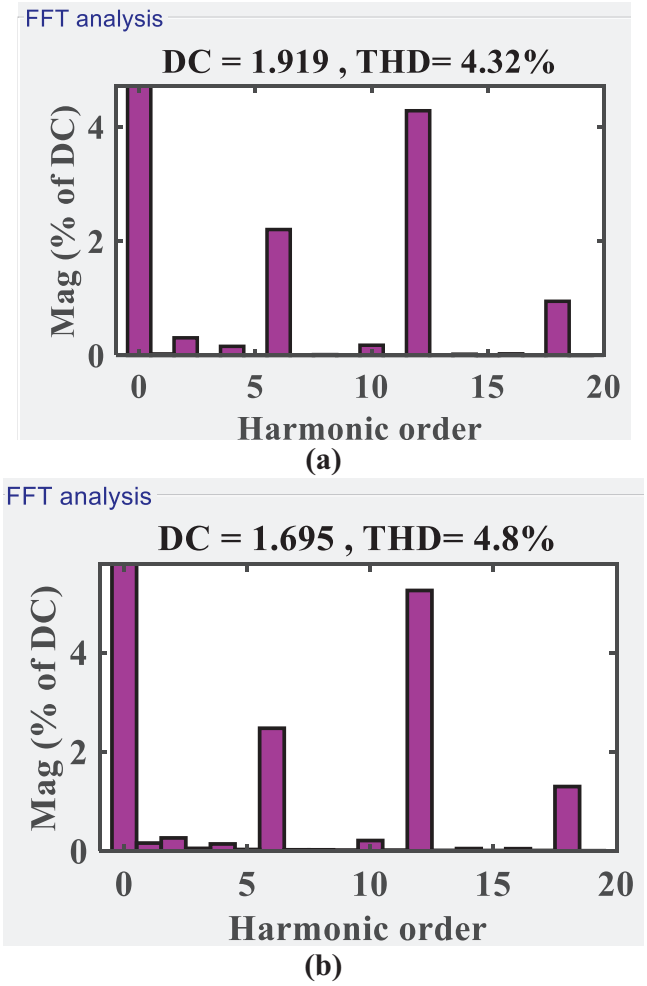

FIGURE 20 The harmonic spectrum of the 7th component current when using HD-DDSRF method: (a) *d*-axis, (b) *q*-axis.

TABLE 4 A brief comparison between DSRF and HD-DDSRF.

Method	Complexity	Accuracy	Harmonic filtering capability	Controllability under Unbalanced Conditions
DSRF	Medium	Low	Low	Low
HD-DDSRF	Relatively high	High	High	High

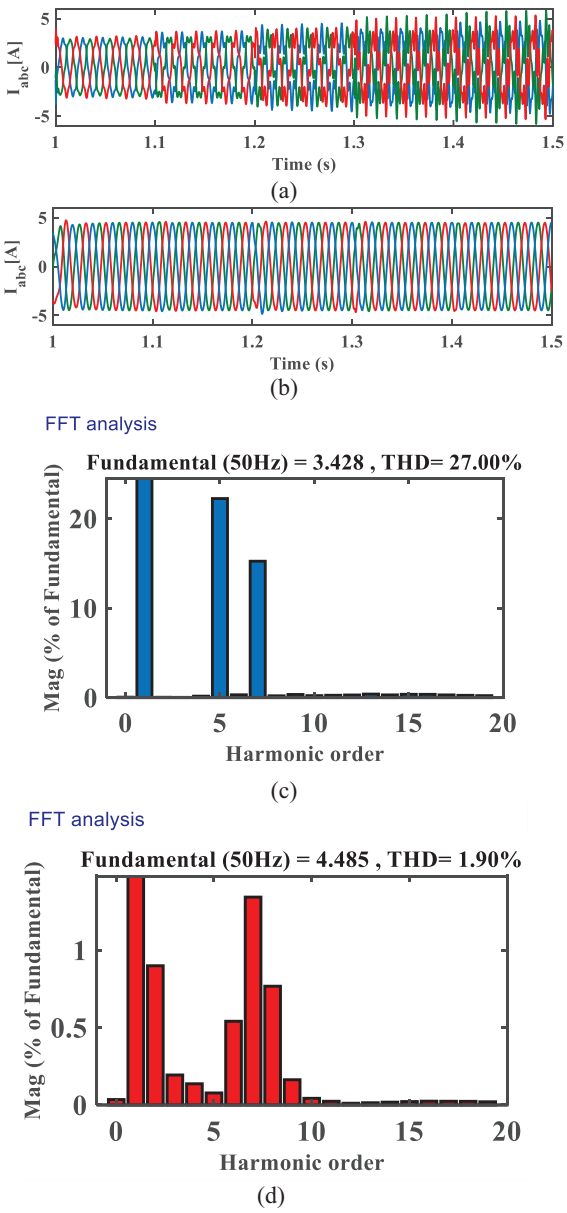

FIGURE 21 Evaluating first harmonic component in *abc* frame. (a) DSRF three-phase waveform, (b) HD-DDSRF three-phase waveform, (c) DSRF THD%, (d) HD-DDSRF THD%.

associated with each approach can be acquired. Table 4 provides a concise comparison of both methods, considering factors such as complexity, accuracy, harmonic filtering capability, and controllability under unbalanced conditions.

While DSRF is relatively simple and computationally efficient, the HD-DDSRF structure is more complex. However, the performance accuracy and harmonic filtering ability of HD-DDSRF are higher than those of DSRF. Additionally, the HD-DDSRF strategy shows excellent controllability when unbalanced conditions like harmonic loads and voltage imbalances occur.

To present future perspectives, since the HD-DDSRF method aims to eliminate the oscillations and create DC signals, it can be employed to eliminate the oscillations of the DC link capacitor when unbalanced conditions exist. Besides separating harmonic components, this method can also be utilized for separating positive and negative components in the presence of both unbalanced and non-linear loads simultaneously.

7 | CONCLUSION

Here, a harmonic detector based on the decoupled double synchronous frame (HD-DDSRF) was employed to detect and

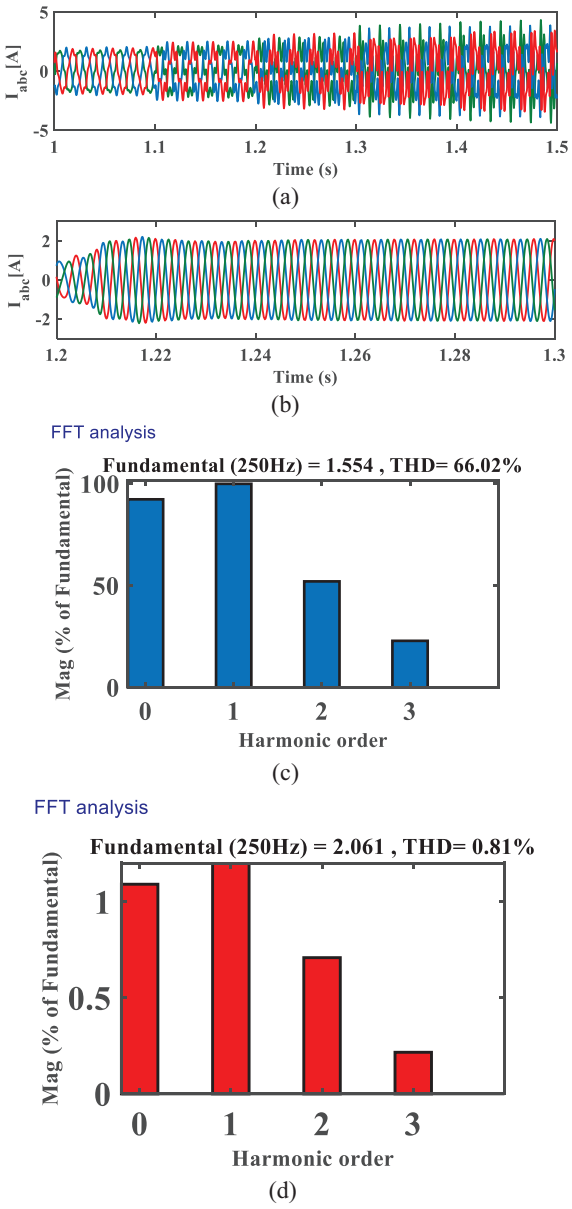

FIGURE 22 Evaluating fifth harmonic component in *abc* frame. (a) DSRF three-phase waveform, (b) HD-DDSRF three-phase waveform, (c) DSRF THD%, (d) HD-DDSRF THD%.

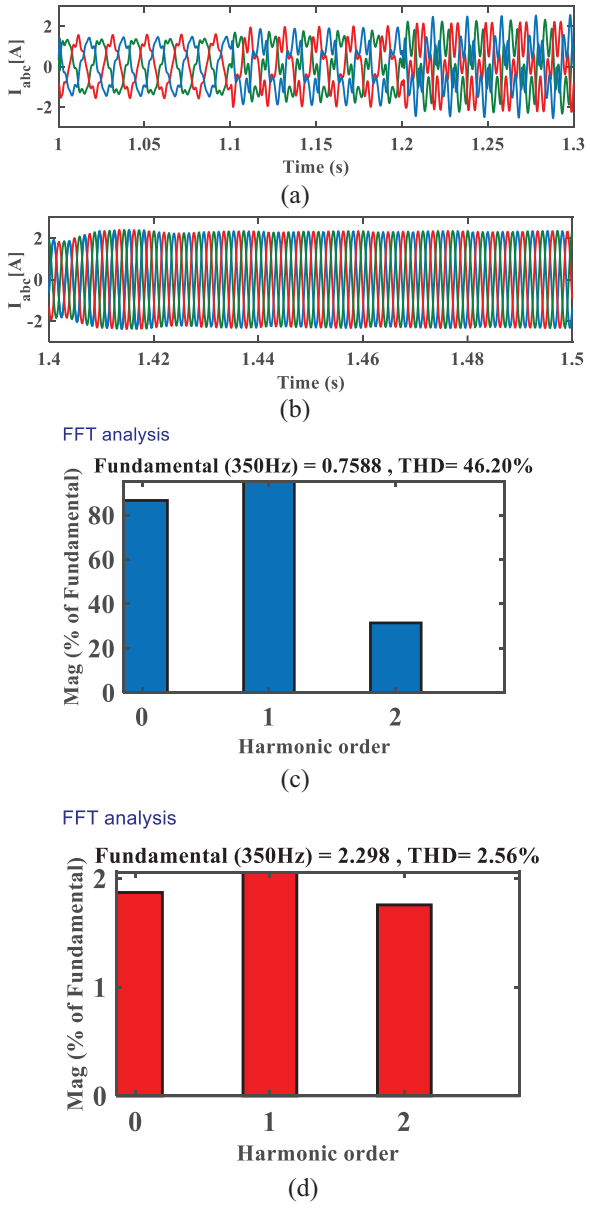

FIGURE 23 Evaluating seventh harmonic component in *abc* frame. (a) DSRF three-phase waveform, (b) HD-DDSRF three-phase waveform, (c) DSRF THD%, (d) HD-DDSRF THD%.

separate the harmonic components and control the current of the main, fifth, and seventh harmonic sequences. The precise mathematical analysis and simulation results showed that the synchronous controller in the *dq* frame, DSRF, malfunctions when harmonic components are injected, and mutual oscillatory couplings appear in the *dq* current. The frequency of these oscillations was proved by using mathematical computations. Additionally, investigating the harmonic spectrum clarified these oscillatory terms. It was also found that the current controller based on the DSRF method could not compensate for fluctuations in any of the references. On the other hand, the results of the HD-DDSRF proposed method showed that the magnitude of DC (MoDC) value was within the acceptable limit and the mutual oscillatory couplings were eliminated by using the HD-DDSRF. In summary, the key findings from simulation scenarios are as below:

- In the first scenario, a comparative simulation was performed to assess the effectiveness of the proposed method. This simulation aimed to highlight the differences between the DSRF and HD-DDSRF methods in mitigating *dq* axis harmonic oscillations. The DSRF detection method exhibited harmonic fluctuations of 38.06%, 37.07%, and 16.46% in the *d*-axis for the main, fifth, and seventh harmonic components, respectively. For the *q*-axis, these fluctuations measured 23.02%, 20.82%, and 75.79%. In contrast, the implementation of the proposed method significantly reduced the amplitude of these fluctuations. Specifically, the *d*-axis harmonic fluctuations

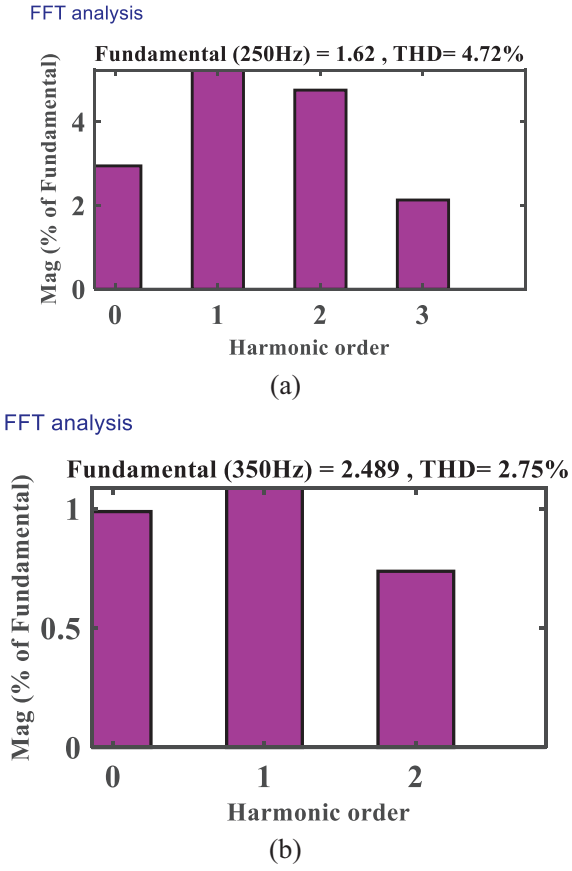

FIGURE 24 Evaluating fifth and seventh harmonic component in *abc* frame for HD-DDSRF method (Scenario B). (a) Fifth harmonic, (b) seventh harmonic.

were minimized to 0.23%, 1.48%, and 0.32% for the main, fifth, and seventh components, respectively. Furthermore, the *q*-axis showed a noticeable reduction, reaching 0.47% for the main component, 0.86% for the fifth component, and 0.77% for the seventh component.

- In the second scenario, having established the effectiveness of the proposed method in comparison with the other approach, we sought to assess its robustness under more challenging conditions. In addition to the prevailing conditions from the first scenario, we introduced a non-linear load to the system. Although the amplitude of harmonic fluctuations increased to some extent, they still remained within an acceptable range, demonstrating the resilience of the proposed method and its ability to maintain satisfactory detection performance even in the presence of non-linear loads.
- Finally, to verify the results obtained from the proposed HD-DDSRF method, comparisons were made with IEEE-519 Standard. The outcome confirms that the THD values for harmonic three-phase waveforms are below the maximum permitted value of (4% THD).

AUTHOR CONTRIBUTIONS

Mojtaba Ahmadi: conceptualization: methodology: software: writing original draft. **Mohammad Hossein Mousavi**: investigation phase: Software: validation: and data curation. **Hassan Moradi**: supervision: reviewing and editing of the manuscript. **Kumars Rouzbehi**: supervision and editing of the manuscript.

CONFLICT OF INTEREST STATEMENT

The authors declare that they have no known competing financial interests or personal relationships that could have appeared to influence the work reported in this paper.

DATA AVAILABILITY STATEMENT

No data applicable.

FUNDING INFORMATION

The authors received no specific funding for this work.

ORCID

Hassan Moradi https://orcid.org/0000-0002-4802-6117
Kumars Rouzbehi https://orcid.org/0000-0002-3623-4840

REFERENCES

1. Dehghani, M., et al.: Control of LPV modeled AC-microgrid based on mixed H2/H∞ time-varying linear state feedback and robust predictive algorithm. IEEE Access 10, 3738–3755 (2022)
2. Fahad, S., Goudarzi, A., Li, Y., Xiang, J.: A coordination control strategy for power quality enhancement of an active distribution network. Energy Rep. 8, 5455–5471 (2022)
3. Wang, X., Blaabjerg, F.: Harmonic stability in power electronic-based power systems: Concept, modelling, and analysis. IEEE Trans. Smart Grid 10(3), 2858–2870 (2018)
4. Li, Y.W., He, J.: Distribution system harmonic compensation methods: An overview of DG-interfacing inverters. IEEE Ind. Electron. Mag. 8(4), 18–31 (2014)
5. Adineh, B., Keypour, R., Davari, P., Blaabjerg, F.: Review of harmonic mitigation methods in microgrid: From a hierarchical control perspective. IEEE J. Emerging Sel. Top. Power Electron. 9(3), 3044–3060 (2020)
6. Mousazadeh Mousavi, S.Y., Jalilian, A., Savaghebi, M., Guerrero, J.M.: Secondary-control-based harmonics compensation scheme for voltage- and current-controlled inverters in islanded microgrids. IET Renewable Power Gener. 14(12), 2176–2182 (2020)
7. Sinvula, R., Abo-Al-Ez, K.M., Kahn, M.T.: Harmonic source detection methods: A systematic literature review. IEEE Access 7, 74283–74299 (2019)
8. Asiminoael, L., Blaabjerg, F., Hansen, S.: Detection is Key-Harmonic detection methods for active power filter applications. IEEE Ind. Appl. Mag. 13(4), 22–33 (2007)
9. Keypour, R., Adineh, B., Khooban, M.H., Blaabjerg, F.: A new population-based optimization method for online minimization of voltage harmonics in islanded microgrids. IEEE Trans. Circuits Syst. II Express Briefs 67(6), 1084–1088 (2019)
10. He, J., Li, Y.W., Guerrero, J.M., Blaabjerg, F., Vasquez, J.C.: An islanding microgrid power sharing approach using enhanced virtual impedance control scheme. IEEE Trans. Power Electron. 28(11), 5272–5282 (2013)
11. Sivakumar, M., Parvathi, R.: Application of neural network trained with meta-heuristic algorithms on fault diagnosis of multi-level inverter. J. Theor. Appl. Inf. Technol. 61(1), 91–98 (2014)
12. Panigrahi, B.K., Senroy, N.: A meta-heuristic approach for optimal classification of power quality disturbances. In: Electric Power Engineering Research and Education, pp. 53–64. Springer, Cham (2015)
13. Iqbal, M., Jawad, M., Jaffery, M.H., Akhtar, S., Rafiq, M.N., Qureshi, M.B., Ansari, A.R., Nawaz, R.: Neural networks-based shunt hybrid active power filter for harmonic elimination. IEEE Access 9, 69913–69925 (2021)
14. Shi, J., Liu, Z.: Harmonic detection technology for power grids based on adaptive ensemble empirical mode decomposition. IEEE Access 9, 21218–21226 (2021)

15. Xiong, L., Zhuo, F., Wang, F., Liu, X., Zhu, M., Yi, H.: A quantitative evaluation and comparison of harmonic elimination algorithms based on moving average filter and delayed signal cancellation in phase synchronization applications. J. Power Electron. 16(2), 717–730 (2016)
16. Chen, D., Lin, Y., Xiao, L., Xu, Z., Lian, H.: A harmonics detection method based on improved comb filter of sliding discrete Fourier for grid-tied inverter. Energy Rep. 6, 1303–1311 (2020)
17. Hoon, Y., Mohd Radzi, M.A., Mohd Zainuri, M.A.A., Zawawi, M.A.M.: Shunt active power filter: A review on phase synchronization control techniques. Electronics 8(7), 791 (2019)
18. Liu, H., Hu, H., Chen, H., Zhang, L., Xing, Y.: Fast and flexible selective harmonic extraction methods based on the generalized discrete Fourier transform. IEEE Trans. Power Electron. 33(4), 3484–3496 (2017)
19. He, J., Li, Y.W., Bosnjak, D., Harris, B.: Investigation and active damping of multiple resonances in a parallel-inverter-based microgrid. IEEE Trans. Power Electron. 28(1), 234–246 (2012)
20. Zhong, Q.C., Blaabjerg, F., Guerrero, J.M., Hornik, T.: Reduction of voltage harmonics for parallel-operated inverters. In: 2011 IEEE Energy Conversion Congress and Exposition. Phoenix, AZ, pp. 473–478 (2011)
21. Micallef, A., Apap, M., Spiteri-Staines, C., Guerrero, J.M.: Cooperative control with virtual selective harmonic capacitance for harmonic voltage compensation in islanded microgrids. In: IECON 2012–38th Annual Conference on IEEE Industrial Electronics Society. Montreal, QC, pp. 5619–5624 (2012)
22. Liu, B., Liu, Z., Liu, J., An, R., Zheng, H., Shi, Y.: An adaptive virtual impedance control scheme based on small-AC-signal injection for unbalanced and harmonic power sharing in islanded microgrids. IEEE Trans. Power Electron. 34(12), 12333–12355 (2019)
23. Pazhanimuthu, C., Baranilingesan, I., Karthick, A.: An improved control algorithm for series hybrid active power filter based on SOGI-PLL under dynamic load conditions. Solid State Commun. 333, 114357 (2021)
24. Tarraso, A., Candela, J.I., Rocabert, J., Rodriguez, P.: Proportional-resonant current controller with orthogonal decoupling on the $\alpha\beta$-reference frame. In: IECON 2017–43rd Annual Conference of the IEEE Industrial Electronics Society. Beijing, China, pp. 1453–1458 (2017)
25. Zhou, S., Liu, J.: Effect of decoupling terms on the performance of PR current controllers implemented in stationary reference frame. In: 2016 IEEE Applied Power Electronics Conference and Exposition (APEC). Long Beach, CA, pp. 3193–3199 (2016)
26. Dash, A.R., Babu, B.C., Mohanty, K.B., Dubey, R.: Analysis of PI and PR controllers for distributed power generation system under unbalanced grid faults. In: 2011 International Conference on Power and Energy Systems. Chennai, India, pp. 1–6 (2011)
27. Rioual, P., Pouliquen, H., Louis, J.P.: Control of a PWM rectifier in the unbalanced state by robust voltage regulation. In: 1993 Fifth European Conference on Power Electronics and Applications. Brighton, UK, pp. 8–14 (1993)
28. Song, H.S., Nam, K.: Dual current control scheme for PWM converter under unbalanced input voltage conditions. IEEE Trans. Ind. Electron. 46(5), 953–959 (1999)
29. Suh, Y., Lipo, T.A.: Control scheme in hybrid synchronous stationary frame for PWM AC/DC converter under generalized unbalanced operating conditions. IEEE Trans. Ind. Appl. 42(3), 825–835 (2006)
30. Cirrincione, M., Pucci, M., Vitale, G., Miraoui, A.: Current harmonic compensation by a single-phase shunt active power filter controlled by adaptive neural filtering. IEEE Trans. Ind. Electron. 56(8), 3128–3143 (2009)
31. Che, Y., Yin, Z., Yu, S., Sun, Q.: Random harmonic detection and compensation based on synchronous reference frame. J. Electr. Comput. Eng. 2017, 7239267 (2017)
32. Reyes, M., Rodriguez, P., Vazquez, S., Luna, A., Teodorescu, R., Carrasco, J.M.: Enhanced decoupled double synchronous reference frame current controller for unbalanced grid-voltage conditions. IEEE Trans. Power Electron. 27(9), 3934–3943 (2012)
33. Li, D., Wang, T., Pan, W., Ding, X., Gong, J.: A comprehensive review of improving power quality using active power filters. Electr. Power Syst. Res. 199, 107389 (2021)
34. Martinek, R., Rzidky, J., Jaros, R., Bilik, P., Ladrova, M.: Least mean squares and recursive least squares algorithms for total harmonic distortion reduction using shunt active power filter control. Energies 12(8), 1545 (2019)
35. Ahmadi, M., Sharafi, P., Mousavi, M.H., Veysi, F.: Power quality improvement in microgrids using statcom under unbalanced voltage conditions. Int. J. Eng. 34(6), 1455–1467 (2021)
36. Li, B., Huang, S., Chen, X., Wan, S.: Enhanced d-q current control for single-phase voltage-source inverters. IET Power Electron. 11(9), 1537–1546 (2018)
37. Prodanović, M., De Brabandere, K., Van den Keybus, J., Green, T., Driesen, J.: Harmonic and reactive power compensation as ancillary services in inverter-based distributed generation. IET Gener. Transm. Distrib. 1(3), 432–438 (2007)
38. Vasquez, J.C., Guerrero, J.M., Savaghebi, M., Eloy-Garcia, J., Teodorescu, R.: Modeling, analysis, and design of stationary-reference-frame droop-controlled parallel three-phase voltage source inverters. IEEE Trans. Ind. Electron. 60(4), 1271–1280 (2012)
39. IEEE Standard for Harmonic Control in Electric Power Systems in IEEE Std 519-2022 (Revision of IEEE Std 519-2014), vol., no., pp. 1–31, 5 Aug. (2022)

How to cite this article: Ahmadi, M., Mousavi, M.H., Moradi, H., Rouzbehi, K.: A new approach for harmonic detection based on eliminating oscillatory coupling effects in microgrids. IET Renew. Power Gener. 17, 3536–3553 (2023).
https://doi.org/10.1049/rpg2.12867

Suppose that the amplitude of 5th and 7th harmonic components are 20% and 10% of the fundamental amplitude, respectively.

$$i_a = \sin(t) + 0.2\sin(5t) + 0.1\sin(7t) \tag{A1}$$

$$i_b = \sin\left(t - \frac{2\pi}{3}\right) + 0.2\sin\left(5t - \frac{2\pi}{3}\right) + 0.1\sin\left(7t - \frac{2\pi}{3}\right) \tag{A2}$$

$$i_c = \sin\left(t + \frac{2\pi}{3}\right) + 0.2\sin\left(5t + \frac{2\pi}{3}\right) + 0.1\sin\left(7t + \frac{2\pi}{3}\right) \tag{A3}$$

Considering Clarke transformation:

$$\begin{bmatrix} i_\alpha \\ i_\beta \end{bmatrix} = \frac{2}{3}\begin{bmatrix} 1 & -\frac{1}{2} & -\frac{1}{2} \\ 0 & \frac{\sqrt{3}}{2} & -\frac{\sqrt{3}}{2} \end{bmatrix}\begin{bmatrix} i_a \\ i_b \\ i_c \end{bmatrix} \tag{A4}$$

If i_a, i_b, and i_c from (A4) are replaced with (A1)–(A3), after simplification, we have:

$$i_\alpha = \frac{2}{15}\sin(5t) + \frac{1}{15}\sin(7t) - \frac{1}{15}\sin\left(5t - \frac{2\pi}{3}\right)$$

$$-\frac{1}{15}\sin\left(5t + \frac{2\pi}{3}\right) - \frac{1}{30}\sin\left(7t - \frac{2\pi}{3}\right) - \frac{1}{30}\left(7t + \frac{2\pi}{3}\right)$$

$$+\frac{2}{3}\sin(t) - \frac{1}{3}\sin\left(t - \frac{2\pi}{3}\right) - \frac{1}{3}\sin\left(t + \frac{2\pi}{3}\right) \tag{A5}$$

$$i_\beta = \frac{1}{3}\left[\frac{\sqrt{3}}{5}\sin\left(5t-\frac{2\pi}{3}\right)+\frac{1}{10}\sin\left(7t-\frac{2\pi}{3}\right)+\sin\left(t-\frac{2\pi}{3}\right)\right]$$

$$-\frac{1}{3}\left[\frac{\sqrt{3}}{5}\sin\left(5t+\frac{2\pi}{3}\right)+\frac{1}{10}\sin\left(7t+\frac{2\pi}{3}\right)+\sin\left(t+\frac{2\pi}{3}\right)\right] \quad \text{(A6)}$$

As can be observed from (A5) and (A6), 1st, 5th, and 7th harmonic orders are appeared in $\alpha\beta$ frame.